Automatica 44 (2008) 2498–2507

Contents lists available at ScienceDirect

Automatica

journal homepage: www.elsevier.com/locate/automatica

# MHD channel flow control in 2D: Mixing enhancement by boundary feedback☆

Eugenio Schuster [a,*], Lixiang Luo [a], Miroslav Krstić [b]

[a] Department of Mechanical Engineering and Mechanics, Lehigh University, Bethlehem, PA 18015-1835, United States

[b] Department of Mechanical and Aerospace Engineering, University of California at San Diego, La Jolla, CA 92093-0411, United States

ARTICLE INFO

*Article history:*
Received 5 July 2006
Received in revised form
5 February 2008
Accepted 14 February 2008
Available online 19 September 2008

*Keywords:*
MHD flow control
Nonlinear boundary control
Active mixing enhancement
Distributed parameter systems

ABSTRACT

A nonlinear Lyapunov-based boundary feedback control law is proposed for mixing enhancement in a 2D magnetohydrodynamic (MHD) channel flow, also known as Hartmann flow, which is electrically conducting, incompressible, and subject to an external transverse magnetic field. The MHD model is a combination of the Navier–Stokes PDE and the Magnetic Induction PDE, which is derived from the Maxwell equations. Pressure sensors, magnetic field sensors, and micro-jets embedded into the walls of the flow domain are employed for mixing enhancement feedback. The proposed control law, designed using passivity ideas, is optimal in the sense that it maximizes a measure related to mixing (which incorporates stretching and folding of material elements), while at the same time minimizing the control and sensing efforts. A DNS code is developed, based on a hybrid Fourier pseudospectral-finite difference discretization and the fractional step technique, to numerically assess the controller.



## 1. Introduction

Recent years have been marked by dramatic advances in active flow control (see Aamo and Krstic (2002) and the references therein), which, if implemented through micro-electro-mechanical sensors and actuators, can become effective in reducing drag and separation over aircraft wings, eliminating instabilities in various sections of jet engines (inlet, compressor rotating stall, combustion thermoacoustic oscillations, etc.), reducing jet noise, reducing thermal signature of jet exhaust through actively controlled mixing, and steering the overall vehicle.

Up until now active feedback flow control developments have had little impact on electrically conducting fluids moving in electromagnetic fields. Active feedback control in electrically conducting flows, implemented through micro-electro-mechanical or micro-electro-magnetic actuators and sensors, can be used to optimally achieve the desired level of stability (when suppression of turbulence is desired) or instability (when enhancement of mixing is desired). As a result, a small amount of active control applied to magnetohydrodynamic (MHD) flows, magnetogasdynamic (MGD) flows, and plasma flows can dramatically change their equilibrium profiles and stability (turbulent fluctuation) properties. These changes influence heat transfer, hydrodynamic drag, pressure drop, and the pumping power required to drive the fluid.

Prior work in the area of active control of electrically-conducting-fluid flows focuses mainly on electro-magneto-hydrodynamic (EMHD) flow control for hydrodynamic drag reduction, through turbulence control, in weak electrically conducting fluids such as saltwater. Traditionally two types of actuator designs have been used: one type generates a Lorentz field parallel to the wall in the streamwise direction, while the other type generates a Lorentz field normal to the wall in the spanwise direction. EMHD flow control has been dominated by *open-loop* strategies that either permanently activate the actuators or pulse them at arbitrary frequencies. However, it has been shown that *feedback* control schemes can improve the efficiency, by reducing control power, for both streamwise (Spong, Reizes, & Leonardi, 2005) and spanwise (Berger, Kim, Lee, & Lim, 2000; Choi, Moin, & Kim, 1994) approaches. Model-based designs for electromagnetically actuated control for drag reduction have been proposed, using distributed control techniques based on linearization and model reduction, in Baker, Armaou, and Christofides (2002); Singh and Bandyopadhyay (1997).

We consider a novel flow control problem that arises when an electrically conducting fluid interacts with a magnetic field in applications that range from liquid metals to plasmas. When an electrically conducting fluid moves in the presence of a transverse magnetic field, it produces an electric field due to charge separation and subsequently an electric current. The interaction between this created electric current and the imposed magnetic field produces a body force, called the Lorentz force, which acts on the fluid itself. Since this force acts in the opposite direction of the

☆ This paper was not presented at any IFAC meeting. This paper was recommended for publication in revised form by Associate Editor Denis Dochain under the direction of Editor Frank Allgöwer. Supported by the Pennsylvania Infrastructure Technology Alliance and the NSF CAREER program (ECCS-0645086).

* Corresponding author. Tel.: +1 610 758 5253.
*E-mail address:* schuster@lehigh.edu (E. Schuster).

0005-1098/$ – see front matter © 2008 Elsevier Ltd. All rights reserved.
doi:10.1016/j.automatica.2008.02.018

fluid motion, a high increase of power becomes necessary to drive the fluid. In addition, this force tends to suppress turbulence and laminarize the flow, which is undesirable in applications where a high rate of heat transfer is needed. The heat transfer decrease due to the laminarization may prevent electrically-conducting-fluid-based cooling systems from producing the heat transfer improvements expected based on the high thermal conductivity of the coolant. Active control can be used to enhance turbulence, mixing, and therefore heat transfer.

We focus in this paper on mixing enhancement by feedback in MHD flows. We consider the *Hartmann flow*, an electrically conducting, incompressible fluid moving between parallel plates through an imposed transverse magnetic field, and extend boundary control design ideas for Navier–Stokes equations (Aamo, Krstić, & Bewley, 2003; Balogh, Aamo, & Krstic, 2005) to MHD flows. Micro-jets, pressure sensors, and magnetic field sensors embedded into the walls of the flow domain would be employed to implement our feedback control law. We develop a direct numerical simulation (DNS) code based on a hybrid Fourier pseudospectral-finite difference discretization scheme and the fractional step technique, and employ it to assess the effectiveness of the proposed controller in a 2D MHD channel flow. The global mathematical well posedness of MHD equations was established in Chen and Wang (2002) for a free boundary problem. The local exact controllability was studied in Barbu, Havarneanu, Popa, and Sritharan (2005).

The paper is organized as follows. Section 2 and 3 introduces the governing equations and their equilibrium solution. The perturbation equations are introduced in Section 4. The Lyapunov analysis and the statement of optimality for the boundary control law is presented in Section 5. In Section 6 the numerical method used to simulate the MHD channel flow is described. Results of an extensive simulation study are presented in Section 7. Section 8 states the conclusions.

## 2. Governing equations

Let us consider the flow of an incompressible, conducting fluid between parallel plates where a magnetic field $\mathbf{B_o} = B_o\hat{\mathbf{y}}$ perpendicular to the channel axis is externally applied. In addition, let us assume the presence of a uniform pressure gradient in the $-\hat{\mathbf{x}}$ direction. Fig. 1 illustrates the configuration; $\hat{\mathbf{x}}$ and $\hat{\mathbf{y}}$ denote the unit vectors in the $x$ and $y$ directions respectively. This flow was first investigated experimentally and theoretically by Hartmann (1937). The governing equations for the stated problem are the transport equation of linear momentum

$$\rho\left[\frac{\partial \mathbf{v}}{\partial t} + (\mathbf{v}\cdot\nabla)\mathbf{v}\right] = -\nabla P + \rho\nu\nabla^2\mathbf{v} + \mathbf{j}\times\mathbf{B}, \tag{1}$$

and the transport equation of magnetic induction

$$\frac{\partial \mathbf{B}}{\partial t} + (\mathbf{v}\cdot\nabla)\mathbf{B} = \frac{1}{\mu\sigma}\nabla^2\mathbf{B} + (\mathbf{B}\cdot\nabla)\mathbf{v}. \tag{2}$$

The flow velocity is denoted by $\mathbf{v}$, the magnetic field by $\mathbf{B}$ and the current density by $\mathbf{j}$, while $P$ denotes the pressure, $\rho$ the fluid mass density, $\nu$ the kinematic viscosity, $\mu$ the magnetic permeability and $\sigma$ the electrical conductivity. The $\mathbf{j}\times\mathbf{B}$ term represents the Lorentz forces. The Lorentz forces couple the mechanical and electrodynamic states of the system and act in planes perpendicular to both current density and magnetic field vectors. Coulomb forces $q\mathbf{E}$, where $q$ is the electrical charge and $\mathbf{E}$ the electrical field, are negligible in comparison to the Lorentz forces. The magnetic induction equation is derived from Ohm's law $\mathbf{j} = \sigma(\mathbf{E} + \mathbf{v}\times\mathbf{B})$, Faraday's law $\frac{\partial \mathbf{B}}{\partial t} = -\nabla\times\mathbf{E}$, Ampere's law $\mu\mathbf{j} = \nabla\times\mathbf{B}$, and the fact that $\mathbf{B}$ and $\mathbf{v}$ are solenoidal $\nabla\cdot\mathbf{B} = 0$, $\nabla\cdot\mathbf{v} = 0$.

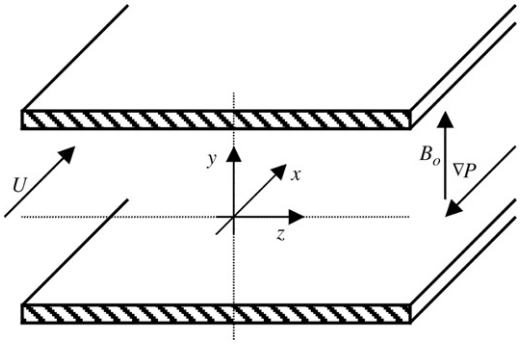


**Fig. 1.** Flow between parallel plates in the presence of a transverse magnetic field (Hartmann flow).

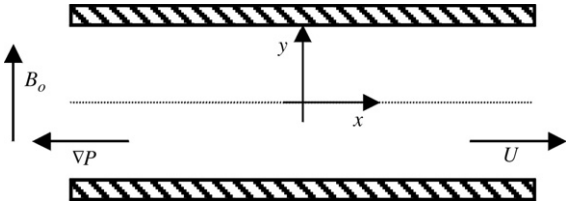


**Fig. 2.** 2D Hartmann flow.

In this work we consider the 2D Hartmann flow. Fig. 2 shows the geometrical arrangement, where $-L \le y \le L$, $-\infty < x < \infty$. The imposed magnetic field $\mathbf{B_o}$ is perpendicular to both planes. In this case we can write $\mathbf{x} = x\hat{\mathbf{x}} + y\hat{\mathbf{y}}$, $\mathbf{v} = \mathbf{v}(x, y, t) = U(x, y, t)\hat{\mathbf{x}} + V(x, y, t)\hat{\mathbf{y}}$, $\mathbf{B} = \mathbf{B}(x, y, t) = B^u(x, y, t)\hat{\mathbf{x}} + B^v(x, y, t)\hat{\mathbf{y}}$ and $P = P(x, y, t)$.

## 3. Equilibrium solution

For channels with constant cross section, as the one depicted in Fig. 2, a fully developed equilibrium flow is established. In this case, the flow velocity $\bar{\mathbf{v}} = \bar{U}(y)\hat{\mathbf{x}}$ has only one component, which depends on the coordinate $y$ (the upper bar denotes equilibrium variables). The magnetic field is decomposed into two contributions, one due to the external imposed magnetic field and the other caused by the magnetic field induced by the flow $\bar{\mathbf{B}} = \mathbf{B_o} + \bar{\mathbf{b}} = B_o\hat{\mathbf{y}} + \bar{\mathbf{b}}$. Substituting this expression for the equilibrium magnetic field $\bar{\mathbf{B}}$ into Eq. (2), and forcing the temporal derivative to zero, shows that the only component of the induced magnetic field is $\bar{\mathbf{b}} = \bar{b}(y)\hat{\mathbf{x}}$. The induction equation reduces then to

$$0 = \mu\sigma B_o\frac{\mathrm{d}\bar{U}}{\mathrm{d}y} + \frac{\mathrm{d}^2\bar{b}}{\mathrm{d}y^2}. \tag{3}$$

Using Ampere's law it is possible to write the current density $\bar{\mathbf{j}}$, and consequently the Lorentz force $\bar{\mathbf{j}}\times\bar{\mathbf{B}}$, in terms of $\bar{b}$. Then the momentum equation can be written as

$$0 = -\frac{\mathrm{d}\bar{P}}{\mathrm{d}x} + \frac{B_o}{\mu}\frac{\mathrm{d}\bar{b}}{\mathrm{d}y} + \rho\nu\frac{\mathrm{d}^2\bar{U}}{\mathrm{d}y^2}. \tag{4}$$

We consider viscous fluids with no slip at the fluid-wall interface $\Gamma$. Therefore the hydrodynamic boundary condition is

$$\bar{\mathbf{v}} = 0 \quad \text{at } \Gamma, \tag{5}$$

which means that all the velocity components vanish at the wall. For walls with finite electrical conductivity $\sigma_w$, magnetic permeability $\mu_w$ and normal $\mathbf{n}$, the condition that the tangential component of the electrical field is continuous across the wall interface can be expressed in terms of $\bar{b}$ as Müller and Bühler (2001)

$$\frac{\partial\bar{b}}{\partial n} - \frac{1}{c}\bar{b} = 0 \quad \text{at } \Gamma, \tag{6}$$

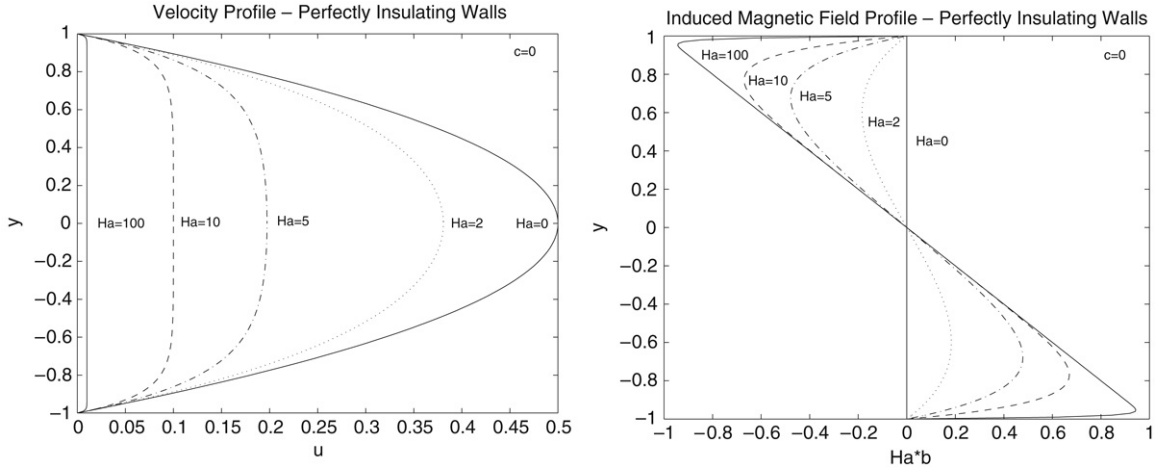


**Fig. 3.** Velocity and induced magnetic field profiles for Hartmann flow at Hartmann numbers $Ha = 0, 2, 5, 10, 100$ for perfectly insulating walls ($c = 0$).

with the wall conductance ratio defined as $c = \frac{\mu_w \sigma_w t_w}{\mu \sigma L}$ where the wall thickness $t_w$ is often small compared to the dimension of the cross section $L$. Two limiting cases can be considered: i- $\bar{b} = 0$ at $\Gamma$ as $c \to 0$ (perfectly insulating walls), ii- $\frac{\partial \bar{b}}{\partial n} = 0$ at $\Gamma$ as $c \to \infty$ (perfectly conducting walls).

Defining the dimensionless variables $y^* = \frac{y}{x_o}$, $\bar{U}^* = \frac{\bar{U}}{v_o}$, $\bar{b}^* = \frac{\bar{b}}{b_o}$, where $x_o = L$, $v_o = \frac{L^2}{\rho \nu}(-\frac{\partial \bar{P}}{\partial x})$, and $b_o = \mu L^2 \sqrt{\frac{\sigma}{\rho \nu}}(-\frac{\partial \bar{P}}{\partial x})$, we can rewrite Eqs. (3) and (4) as

$$Ha \frac{\mathrm{d}\bar{U}^*}{\mathrm{d}y^*} + \frac{\mathrm{d}^2 \bar{b}^*}{\mathrm{d}y^{*2}} = 0, \qquad Ha \frac{\mathrm{d}\bar{b}^*}{\mathrm{d}y^*} + \frac{\mathrm{d}^2 \bar{U}^*}{\mathrm{d}y^{*2}} = -1, \tag{7}$$

with boundary conditions (5) and (6) now expressed as

$$\begin{aligned} &\bar{U}^* = 0 \quad \text{at } y^* = \pm 1 \\ &\mp \frac{\mathrm{d}\bar{b}^*}{\mathrm{d}y^*} - \frac{\bar{b}^*}{c} = 0 \quad \text{at } y^* = \pm 1, \end{aligned} \tag{8}$$

where $Ha = B_o L \sqrt{\frac{\sigma}{\rho \nu}}$ is the Hartmann number. The solution for system (7) with boundary conditions (8) is given by

$$\bar{U}^*(y^*) = \frac{1}{Ha} \frac{c+1}{cHa + \tanh(Ha)} \left[ 1 - \frac{\cosh(Ha\, y^*)}{\cosh(Ha)} \right], \tag{9}$$

$$\bar{b}^*(y^*) = -\frac{y^*}{Ha} + \frac{1}{Ha} \frac{c+1}{cHa + \tanh(Ha)} \frac{\sinh(Ha\, y^*)}{\cosh(Ha)}. \tag{10}$$

Fig. 3 shows the velocity and induced magnetic field profiles for different values of the Hartmann number $Ha$ in the case of perfectly insulating walls, $c = 0$.

## 4. Perturbation equations

Defining the dimensionless variables $\mathbf{x}^* = \frac{\mathbf{x}}{x_o}$, $\mathbf{v}^* = \frac{\mathbf{v}}{v_o}$, $t^* = \frac{v_o t}{x_o}$, $\mathbf{B}^* = \frac{\mathbf{B}}{b_o}$, $\mathbf{j}^* = \frac{\mathbf{j}}{\sigma v_o b_o}$, with $x_o$, $v_o$, and $b_o$ defined in the previous section, we can rewrite Eqs. (1) and (2) as

$$\frac{\partial \mathbf{v}}{\partial t} + (\mathbf{v} \cdot \nabla)\mathbf{v} = -\nabla P + \frac{1}{R} \nabla^2 \mathbf{v} + \frac{N}{R_m} [(\nabla \times \mathbf{B}) \times \mathbf{B}], \tag{11}$$

$$\frac{\partial \mathbf{B}}{\partial t} + (\mathbf{v} \cdot \nabla)\mathbf{B} = \frac{1}{R_m} \nabla^2 \mathbf{B} + (\mathbf{B} \cdot \nabla)\mathbf{v}, \tag{12}$$

where $R = \frac{v_o L}{\nu}$ is the Reynolds number, $N = \frac{\sigma L b_o^2}{\rho v_o}$ is the Stuart number, and $R_m = \mu \sigma v_o L$ is the magnetic Reynolds number. The star notation has been dropped for simplicity.

Defining the deviation variables as $u = U - \bar{U}$, $v = V - \bar{V} = V$, $b^u = B^u - \bar{B}^u = B^u - \bar{b}$, $b^v = B^v - \bar{B}^v = B^v - B_o$, $p = P - \bar{P}$, we can write the dimensionless perturbation equations as

$$\begin{aligned} &\frac{\partial u}{\partial t} + (\bar{U} + u)\frac{\partial u}{\partial x} + v \frac{\partial (\bar{U} + u)}{\partial y} = -\frac{\partial p}{\partial x} + \frac{1}{R}\left( \frac{\partial^2 u}{\partial x^2} + \frac{\partial^2 u}{\partial y^2} \right) \\ &\quad - \frac{N}{R_m}(B_o + b^v)\left( \frac{\partial b^v}{\partial x} - \frac{\partial b^u}{\partial y} \right) + \frac{N}{R_m} b^v \frac{\partial \bar{b}}{\partial y}, \end{aligned} \tag{13}$$

$$\begin{aligned} &\frac{\partial v}{\partial t} + (\bar{U} + u)\frac{\partial v}{\partial x} + v \frac{\partial v}{\partial y} = -\frac{\partial p}{\partial y} + \frac{1}{R}\left( \frac{\partial^2 v}{\partial x^2} + \frac{\partial^2 v}{\partial y^2} \right) \\ &\quad + \frac{N}{R_m}(\bar{b} + b^u)\left( \frac{\partial b^v}{\partial x} - \frac{\partial b^u}{\partial y} \right) - \frac{N}{R_m} b^u \frac{\partial \bar{b}}{\partial y}, \end{aligned} \tag{14}$$

$$\frac{\partial u}{\partial x} + \frac{\partial v}{\partial y} = 0, \tag{15}$$

$$\begin{aligned} &\frac{\partial b^u}{\partial t} + (\bar{U} + u)\frac{\partial b^u}{\partial x} + v \frac{\partial (\bar{b} + b^u)}{\partial y} = \frac{1}{R_m}\left( \frac{\partial^2 b^u}{\partial x^2} + \frac{\partial^2 b^u}{\partial y^2} \right) \\ &\quad + (\bar{b} + b^u)\frac{\partial u}{\partial x} + (B_o + b^v)\frac{\partial u}{\partial y} + b^v \frac{\partial U}{\partial y}, \end{aligned} \tag{16}$$

$$\begin{aligned} &\frac{\partial b^v}{\partial t} + (\bar{U} + u)\frac{\partial b^v}{\partial x} + v \frac{\partial b^v}{\partial y} = \frac{1}{R_m}\left( \frac{\partial^2 b^v}{\partial x^2} + \frac{\partial^2 b^v}{\partial y^2} \right) \\ &\quad + (\bar{b} + b^u)\frac{\partial v}{\partial x} + (B_o + b^v)\frac{\partial v}{\partial y}, \end{aligned} \tag{17}$$

$$\frac{\partial b^u}{\partial x} + \frac{\partial b^v}{\partial y} = 0, \tag{18}$$

with initial conditions $u(x, y, 0) = u_o(x, y)$, $v(x, y, 0) = v_o(x, y)$, $b^u(x, y, 0) = b_o^u(x, y)$, $b^v(x, y, 0) = b_o^v(x, y)$ for $-\infty < x < \infty$, $-1 < y < 1$ and $t > 0$.

## 5. Energy analysis, control design, and its inverse optimality

Choosing the energy function as the combination of the perturbed kinetic and magnetic energies of the flow,

$$E(\mathbf{v}, \mathbf{B}) = \frac{1}{2} \int_{-1}^{1} \int_{0}^{d} k_1 (u^2 + v^2) + k_2 (b^{u^2} + b^{v^2}) \mathrm{d}x\mathrm{d}y, \tag{19}$$

we can compute

$$\dot{E}(\mathbf{v}, \mathbf{B}) = \int_{-1}^{1} \int_{0}^{d} (k_1 u u_t + k_1 v v_t + k_2 b^u b_t^u + k_2 b^v b_t^v) \mathrm{d}x\mathrm{d}y$$

$$
\begin{aligned}
&= k_1 \int_{-1}^{1}\int_0^d -u\left[\bar{U}u_x + uu_x + v\bar{U}' + vu_y - \frac{1}{R}\left(u_{xx}+u_{yy}\right) + p_x\right]\mathrm{d}x\mathrm{d}y\\
&\quad + k_1 \int_{-1}^{1}\int_0^d -u\left[\frac{N}{R_m}B_o\left(b_x^v - b_y^u\right) + \frac{N}{R_m}b^v\left(b_x^v - b_y^u\right) - \frac{N}{R_m}b^v\bar{b}'\right]\mathrm{d}x\mathrm{d}y\\
&\quad + k_1 \int_{-1}^{1}\int_0^d -v\left[\bar{U}v_x + uv_x + vv_y - \frac{1}{R}\left(v_{xx}+v_{yy}\right) + p_y\right]\mathrm{d}x\mathrm{d}y\\
&\quad + k_1 \int_{-1}^{1}\int_0^d -v\left[-\frac{N}{R_m}\bar{b}\left(b_x^v - b_y^u\right) - \frac{N}{R_m}b^u\left(b_x^v - b_y^u\right) + \frac{N}{R_m}b^u\bar{b}'\right]\mathrm{d}x\mathrm{d}y\\
&\quad + k_2 \int_{-1}^{1}\int_0^d -b^u\left[\bar{U}b_x^u + ub_x^u + v\bar{b}' + vb_y^u - \frac{1}{R_m}\left(b_{xx}^u + b_{yy}^u\right)\right]\mathrm{d}x\mathrm{d}y\\
&\quad + k_2 \int_{-1}^{1}\int_0^d -b^u\left[-\bar{b}u_x - b^u u_x - B_o u_y - b^v u_y - b^v\bar{U}'\right]\mathrm{d}x\mathrm{d}y\\
&\quad + k_2 \int_{-1}^{1}\int_0^d -b^v\left[\bar{U}b_x^v + ub_x^v + vb_y^v - \frac{1}{R_m}\left(b_{xx}^v + b_{yy}^v\right)\right]\mathrm{d}x\mathrm{d}y\\
&\quad + k_2 \int_{-1}^{1}\int_0^d -b^v\left[-\bar{b}v_x - b^u v_x - B_o v_y - b^v v_y\right]\mathrm{d}x\mathrm{d}y, \qquad (20)
\end{aligned}
$$

where $\bar{U}'$ and $\bar{b}'$ denote $\bar{U}_y$ and $\bar{b}_y$ respectively. We assume periodic boundary conditions in the streamwise direction, i.e., $\mathbf{v}(x=0) = \mathbf{v}(x=d)$, $\mathbf{B}(x=0) = \mathbf{B}(x=d)$ and $p(x=0) = p(x=d)$. We apply control only in the wall normal direction, i.e.,

$$u(x,-1,t) = u(x,1,t) = 0, \qquad (21)$$

$$v(x,-1,t) = v(x,1,t) = v_{\mathrm{wall}}(x,t), \qquad (22)$$

where the control $v_{\mathrm{wall}}(x,t)$, to be employed on both the top and the bottom walls, is to be designed. Note that (22) ensures that the net mass flux through the walls be zero. We measure the wall normal component of the induced magnetic field,

$$b^u(x,-1,t) = b^u(x,1,t) = 0, \qquad (23)$$

$$b^v(x,-1,t) = b^v_{\mathrm{bot\_wall}}(x,t),\ b^v(x,1,t) = b^v_{\mathrm{top\_wall}}(x,t), \qquad (24)$$

where $b^v_{\mathrm{bot\_wall}}(x,t)$ and $b^v_{\mathrm{bot\_wall}}(x,t)$ are measured on the bottom and top wall, respectively, and (23) follows from assuming perfectly insulating walls.

**Lemma 1.** *Taking into account boundary conditions (21)–(24) the time derivative of $E(\mathbf{v},\mathbf{B})$ along the trajectories can be written as*

$$
\begin{aligned}
\dot{E}(\mathbf{v},\mathbf{B}) &= -\frac{1}{R}m(\mathbf{v},\mathbf{B}) - \int_0^d v_{\mathrm{wall}}\left[k_1\Delta p + k_2\frac{\Delta\left(b^{v^2}\right)}{2}\right]\mathrm{d}x\\
&\quad + g(\mathbf{v},\mathbf{B}), \qquad (25)
\end{aligned}
$$

*where*

$$
\begin{aligned}
m(\mathbf{v},\mathbf{B}) &= k_1\int_{-1}^{1}\int_0^d (u_x^2 + u_y^2 + v_x^2 + v_y^2)\mathrm{d}x\mathrm{d}y\\
&\quad + k_2\frac{R}{R_m}\int_{-1}^{1}\int_0^d \left((b_x^u)^2 + (b_y^u)^2 + (b_x^v)^2 + (b_y^v)^2\right)\mathrm{d}x\mathrm{d}y, \qquad (26)
\end{aligned}
$$

$$
\begin{aligned}
g(\mathbf{v},\mathbf{B}) &= -k_1\int_{-1}^{1}\int_0^d \bar{U}'uv\,\mathrm{d}x\mathrm{d}y \qquad (27)\\
&\quad - k_2\int_{-1}^{1}\int_0^d \bar{b}'b^u v\,\mathrm{d}x\mathrm{d}y \qquad (28)\\
&\quad + k_2\int_{-1}^{1}\int_0^d \bar{U}'b^u b^v\,\mathrm{d}x\mathrm{d}y \qquad (29)\\
&\quad + k_1\int_{-1}^{1}\int_0^d \frac{N}{R_m}\bar{b}'\left(ub^v - vb^u\right)\mathrm{d}x\mathrm{d}y \qquad (30)\\
&\quad + k_1\int_{-1}^{1}\int_0^d \frac{N}{R_m}\bar{b}\left(b_x^v - b_y^u\right)v\,\mathrm{d}x\mathrm{d}y \qquad (31)\\
&\quad - k_1\int_{-1}^{1}\int_0^d \frac{N}{R_m}B_o\left(b_x^v - b_y^u\right)u\mathrm{d}x\mathrm{d}y \qquad (32)\\
&\quad + k_2\int_{-1}^{1}\int_0^d \bar{b}\left(b^u u_x + b^v v_x\right)\mathrm{d}x\mathrm{d}y \qquad (33)\\
&\quad + k_2\int_{-1}^{1}\int_0^d B_o\left(b^u u_y + b^v v_y\right)\mathrm{d}x\mathrm{d}y \qquad (34)\\
&\quad + k_1\int_{-1}^{1}\int_0^d \frac{N}{R_m}b^u\left(b_x^v - b_y^u\right)v\mathrm{d}x\mathrm{d}y \qquad (35)\\
&\quad - k_1\int_{-1}^{1}\int_0^d \frac{N}{R_m}b^v\left(b_x^v - b_y^u\right)u\mathrm{d}x\mathrm{d}y \qquad (36)\\
&\quad + k_2\int_{-1}^{1}\int_0^d b^u b^u u_x\mathrm{d}x\mathrm{d}y \qquad (37)\\
&\quad + k_2\int_{-1}^{1}\int_0^d b^u b^v v_x\mathrm{d}x\mathrm{d}y \qquad (38)\\
&\quad + k_2\int_{-1}^{1}\int_0^d b^v b^u u_y\mathrm{d}x\mathrm{d}y \qquad (39)\\
&\quad + k_2\int_{-1}^{1}\int_0^d b^v b^v v_y\mathrm{d}x\mathrm{d}y, \qquad (40)
\end{aligned}
$$

$$\Delta p = P(x,1,t) - P(x,-1,t), \qquad (41)$$

$$\Delta\left(b^{v^2}\right) = (b^v(x,1,t))^2 - (b^v(x,-1,t))^2. \qquad (42)$$

This lemma, proved in Appendix A, provides a relationship between the time derivative of $E(\mathbf{v},\mathbf{B})$ and the function $m(\mathbf{v},\mathbf{B})$, which appears to be connected to mixing. A number of inherently different processes is called mixing. Ottino (1989) distinguishes sub-problems of mixing: (i) mixing of a single fluid (or similar fluids) governed by the stretching and folding of material elements; (ii) mixing governed by diffusion or chemical reactions; and (iii) mixing of different fluids governed by the breakup and coalescence of material elements. Of course, all processes may be present simultaneously. In this work, we are interested in the first sub-problem. The measure (26) is related to mixing due to the direct correspondence between stretching of material elements and the spatial gradients of the flow field. Folding is present implicitly in (26) due to the boundedness of the flow domain and the fact that $\mathbf{v}$ satisfies the Navier–Stokes equation. In this first sub-problem, the interfaces between the fluids are passive (Aref & Tryggvason, 1984), and the mixing may be determined by studying the movement of a passive tracer, or dye, in a homogeneous fluid flow. The intuitive correspondence between stretching of material elements and the spatial gradients of the flow field will be further reinforced with our dye simulations. The presence of the spatial derivatives of the induced magnetic field $\mathbf{b}$ in (26) is motivated by the direct relationship between the perturbed induced magnetic field and the perturbed velocity field. The incorporation of the spatial derivatives of the induced magnetic field in (26) is also consistent with the incorporation of the perturbed magnetic energy in (19), and allows for the existence of an elegant solution to the optimal control problem as stated in Theorem 1.

**Lemma 2.** *The function $g(\mathbf{v},\mathbf{B})$ satisfies*

$$|g(\mathbf{v},\mathbf{B})| \le g_1 m(\mathbf{v},\mathbf{B}) + g_2 m^2(\mathbf{v},\mathbf{B}) + g_3\int_0^d v_{\mathrm{wall}}^2\mathrm{d}x + \frac{1}{2}q(\mathbf{v},\mathbf{B}),$$

*where $q(\mathbf{v},\mathbf{B}) = g_4 n + g_5 n^2$, $n(\mathbf{v},\mathbf{B}) = \int_0^d (b^v_{\mathrm{top\_wall}})^2 + (b^v_{\mathrm{bot\_wall}})^2\mathrm{d}x$ and $g_1, g_2, g_3, g_4$ and $g_5$ are nonnegative constants which depend only on the flow parameters.*

This lemma, proved in Appendix B, provides a bound on the crossterm, involving both the perturbation and equilibrium variables, that originates from the nonlinear terms in the MHD equations. This term is similar to the so-called *instantaneous production* term in the fluid mechanics literature.

Our goal is to design a feedback control law, in terms of suction and blowing of fluid normally to the channel wall (achievable by micro-electro-mechanical (MEM) jets (Lofdahl & el Hak, 1999)), that is optimal with respect to some meaningful cost functional related to $m(\mathbf{v}, \mathbf{B})$. The control solution is presented in the following theorem.

**Theorem 1.** *The cost functional*

$$J(v_{\text{wall}}) = \lim_{t\to\infty}\left[2\beta E(\mathbf{v}(t), \mathbf{B}(t)) + \int_0^t h(\mathbf{v}(\tau), \mathbf{B}(\tau))\mathrm{d}\tau\right], \tag{43}$$

*where $\beta > g_3$ is a positive constant and*

$$h(\mathbf{v}, \mathbf{B}) = \frac{2\beta}{R}m(\mathbf{v}, \mathbf{B}) - 2\beta g(\mathbf{v}, \mathbf{B}) - \beta\int_0^d v_{\text{wall}}^2\mathrm{d}x - \beta\int_0^d\left[k_1\Delta p + k_2\frac{\Delta\left(b^{v^2}\right)}{2}\right]^2\mathrm{d}x, \tag{44}$$

*is maximized by the control*

$$v_{\text{wall}} = -\left[k_1\Delta p + k_2\frac{\Delta\left(b^{v^2}\right)}{2}\right]. \tag{45}$$

*Moreover, for arbitrary values of control $v_{\text{wall}}$, solutions of system (13)–(18) satisfy*

$$h(\mathbf{v}, \mathbf{B}) \le l_1 m(\mathbf{v}, \mathbf{B}) + l_2 m^2(\mathbf{v}, \mathbf{B}) + \beta q(\mathbf{v}, \mathbf{B}) - l_3\int_0^d v_{\text{wall}}^2\mathrm{d}x - \beta\int_0^d\left[k_1\Delta p + k_2\frac{\Delta\left(b^{v^2}\right)}{2}\right]^2\mathrm{d}x, \tag{46}$$

$$l_1 = 2\beta\left(\frac{1}{R} + g_1\right), \qquad l_2 = 2\beta g_2, \qquad l_3 = \beta - g_3. \tag{47}$$

**Proof.** By Lemma 1, we can write Eq. (44) as

$$\begin{aligned} h(\mathbf{v}, \mathbf{B}) &= -2\beta\dot{E}(\mathbf{v}, \mathbf{B}) - \beta\int_0^d\left[k_1\Delta p + k_2\frac{\Delta\left(b^{v^2}\right)}{2}\right]^2\mathrm{d}x \\ &\quad - 2\beta\int_0^d v_{\text{wall}}\left[k_1\Delta p + k_2\frac{\Delta\left(b^{v^2}\right)}{2}\right]\mathrm{d}x - \beta\int_0^d v_{\text{wall}}^2\mathrm{d}x \\ &= -2\beta\dot{E}(\mathbf{v}, \mathbf{B}) - \beta\int_0^d\left(v_{\text{wall}} + \left[k_1\Delta p + k_2\frac{\Delta\left(b^{v^2}\right)}{2}\right]\right)^2\mathrm{d}x, \end{aligned} \tag{48}$$

and the cost functional can be written as

$$\begin{aligned} J(v_{\text{wall}}) &= \lim_{t\to\infty}\Bigg[2\beta E(\mathbf{v}(t), \mathbf{B}(t)) - 2\beta\int_0^t\dot{E}(\mathbf{v}(\tau), \mathbf{B}(\tau))\mathrm{d}\tau \\ &\quad -\beta\int_0^t\int_0^d\left(v_{\text{wall}} + \left[\Delta p + \frac{\Delta\left(b^{v^2}\right)}{2}\right]\right)^2\mathrm{d}x\mathrm{d}\tau\Bigg] \\ &= 2\beta E(\mathbf{v}(0), \mathbf{B}(0)) \\ &\quad -\beta\lim_{t\to\infty}\int_0^t\int_0^d\left(v_{\text{wall}} + \left[k_1\Delta p + k_2\frac{\Delta\left(b^{v^2}\right)}{2}\right]\right)^2\mathrm{d}x\mathrm{d}\tau. \end{aligned} \tag{49}$$

The cost functional (43) is maximized when the last integral in (49) is zero. Therefore the control (45) is optimal. In addition, by Lemma 2 we can write

$$\begin{aligned} h(\mathbf{v}, \mathbf{B}) &\le \frac{2\beta}{R}m(\mathbf{v}, \mathbf{B}) + \beta q(\mathbf{v}, \mathbf{B}) - \beta\int_0^d v_{\text{wall}}^2\mathrm{d}x \\ &\quad -\beta\int_0^d\left[k_1\Delta p + k_2\frac{\Delta\left(b^{v^2}\right)}{2}\right]^2\mathrm{d}x \\ &\quad + 2\beta\left(g_1 m(\mathbf{v}, \mathbf{B}) + g_2 m^2(\mathbf{v}, \mathbf{B}) + g_3\int_0^d v_{\text{wall}}^2\mathrm{d}x\right) \\ &\le l_1 m(\mathbf{v}, \mathbf{B}) + l_2 m^2(\mathbf{v}, \mathbf{B}) + \beta q(\mathbf{v}, \mathbf{B}) \\ &\quad - l_3\int_0^d v_{\text{wall}}^2\mathrm{d}x - \beta\int_0^d\left[k_1\Delta p + k_2\frac{\Delta\left(b^{v^2}\right)}{2}\right]^2\mathrm{d}x. \quad \square \end{aligned}$$

The goal of the control law (45) is to increase the value of $m(\mathbf{v}, \mathbf{B})$. It is clear from inequality (46), which gives an upper bound on $h(\mathbf{v}, \mathbf{B})$ in terms of $m(\mathbf{v}, \mathbf{B})$, that this goal is targeted in the cost functional (43). Inequality (46) implies that $h(\mathbf{v}, \mathbf{B})$ cannot be made large without making the mixing measure $m(\mathbf{v}, \mathbf{B})$ large, so the cost functional (43) is meaningful with respect to our goal. Noting that $\beta > g_3$ implies that $l_3$ is positive (which is not a design choice because $\beta$ is just an analysis constant in the cost functional, whereas the gains $k_1$ and $k_2$ can have arbitrary positive values), we observe that the control law (45) maximizes $J(v_{\text{wall}})$, and therefore $h(\mathbf{v}, \mathbf{B})$, and consequently mixing, with minimal control ($v_{\text{wall}}$) and sensing ($\Delta p$, $\Delta(b^{v^2})$) effort (the cost function (43) also puts penalty on the control and sensing effort through $h(\mathbf{v}, \mathbf{B})$). The only term whose role in (46) is not obvious is $q(\mathbf{v}, \mathbf{B})$. This term is not related to mixing in an obvious way but it is a perturbation variable and, as such, its growth indicates a growth of instability, which contributes to mixing.

The feedback (45) is independent of the parameters of the flow, and thus robust to parameter uncertainties. It requires sensing (of pressure and induced magnetic field) only at the boundary and is decentralized.

## 6. Numerical method

A direct numerical simulation is performed based on the full MHD equations, to allow the measurement of the induced magnetic field at the boundary, as required by the control law (45). Although past research exists on the simulation of the MHD equations for compressible flows, results for unsteady incompressible flows are scarce, due to inherent challenges. The first difficulty is in the multiple time scales—while the momentum equation has $R \gg 1$, the induction equation has $R_m \ll 1$. Secondly, the MHD equations become stiffer as the magnetic Reynolds number decreases. Based on the similar structures of the Navier–Stokes and Magnetic Induction equations, our first approach to the problem was to integrate the equations with different integration steps on a staggered grid within a periodic channel flow geometry using a hybrid Fourier pseudospectral—finite difference discretization and the fractional step technique. Taking advantage of the periodic boundary conditions in the streamwise ($x$) direction, this direction is discretized using Fourier

pseudospectral methods (Canuto, 1998), while the wall-normal ($y$) direction is discretized using central finite differences on a non-uniform staggered grid (Morinishi, Lund, Vasilyev, & Moin, 1998). The equations are integrated in time using a fractional step method (Dukowicz & Dvinsky, 1992), designed to ensure the fulfillment of the divergence-free conditions, based on a hybrid Runge–Kutta/Crank–Nicolson time discretization (Bewley, 1999). Nonlinear terms are integrated explicitly using a fourth-order, low-storage Runge–Kutta method, while linear terms are treated implicitly using the Crank–Nicolson method.

## 7. Simulation results

In this section, the laminarization property of the imposed magnetic field and the effectiveness of the proposed control law (45) for mixing enhancement are studied numerically on the flow domain $-1 < y < 1, 0 < x < 4\pi$, with NX $= 150$ grid points in the $x$ direction and NY $= 128$ grid points in the $y$ direction, and with fixed flow-rate $Q = 1.5$. The tests follow a specific procedure: first, a fully established hydrodynamic flow (no magnetic field) is calculated; second, a magnetic field is imposed on the fully established flow, which leads to another fully established MHD flow with lower perturbation energy or even to a linearly stable MHD flow; finally, boundary feedback is applied to the MHD flow and an increase in the flow complexity is observed and confirmed by the evolution of dye blobs in the flow.

### 7.1. Hydrodynamic channel flow

When $B_o = 0$, the momentum equation (11) reduces to the well-known Navier–Stokes equation. The two-dimensional channel flow, also known as the Poiseuille flow, is frequently cited as a paradigm for transition to turbulence, and has drawn extensive attention through the history of fluid dynamics. This is a classical flow control problem that has been studied in Aamo and Krstic (2002) and the references therein assuming the availability of an array of pressure sensors on the walls and an array of MEMS micro-jet actuators (also distributed along the walls) capable of blowing/suction in the wall-normal direction. Incompressible conventional flows in 2D channels can be stable for low Reynolds numbers, as infinitesimal perturbations in the flow field are damped out. The flows turn linearly unstable for high Reynolds numbers R $> 5772$ (Panton, 1996). Such flows usually reach statistically steady states, which we call fully established flows. The full MHD code is capable of simulating 2D pure hydrodynamic channel flows by simply setting $B_0 = 0$, which means that no magnetic field is imposed. Simulation results are presented in Fig. 4 to show how a channel flow (R $= 7500$) develops to a fully established flow. The initial velocity profile is the parabolic equilibrium solution of the Navier–Stokes equation, which is linearly unstable for this Reynolds number. Fig. 4 shows how the vorticity map evolves in time until reaching a fully established flow when the initial equilibrium velocity profile is infinitesimally perturbed at $t = 0$.

### 7.2. Stabilization effect of the imposed magnetic field in MHD channel flows

When $B_o \neq 0$, Fig. 3 shows that the equilibrium profile is flattened in the center of the channel. In addition, Fig. 5(a) shows the effect of the imposed transverse magnetic field on the stability properties of the flow. Vorticity maps obtained through direct numerical simulation studies show the stabilizing effect of the imposed magnetic field on the 2D Hartmann flow at $t = 140, 285, 374$. The magnetic field is imposed at $t = 0$ with the fully established flow (R $= 7500$) achieved in Fig. 4 for the pure hydrodynamic channel (Section 7.1). Magnetic fields

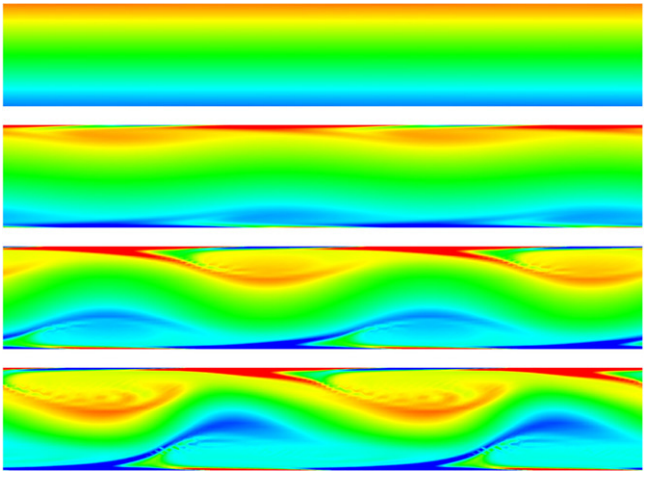

**Fig. 4.** Vorticity maps for R $= 7500$ at $t = 0, 1262, 1682, 4485$, for a pure hydrodynamic channel flow ($B_o = 0$).

of three different levels of strength ($B_0 = 0.1, 0.2, 0.3$) are imposed on the fully established flow at time $t = 0$. The magnetic Reynolds number is $R_m = 0.1$ and the Stuart number is N $= 0.01$ in all cases. Observing the vorticity maps, it is interesting to note that weak magnetic fields (Ha $< 3$) have significant stabilization effects on the fully established flows. Flows with lower Reynolds numbers, with a stronger tendency towards stability, are more easily stabilized by the magnetic fields. The perturbation energy of the velocity field, $E(\mathbf{v}) = \frac{1}{2d}\int_{-1}^{1}\int_{0}^{d}(u^2 + v^2)\mathrm{d}x\mathrm{d}y$, is used to quantify the level of stability/instability of the flow. The time evolutions of perturbation energy are shown in Fig. 5(b). In all cases, the perturbation energy is reduced by the imposed magnetic field, and another fully established flow profile with lower perturbation energy is reached.

### 7.3. Simulations of controlled MHD flow

The controller is started at $t = 0$ with the fully established MHD flow (R $= 7500$, $R_m = 0.1$, N $= 0.01$) shown in Fig. 5(a). The gains of the control are the same for all cases ($k_v = 0.1, k_b = 10{,}000$). The time evolution of the vorticity map is shown for $B_0 = 0.3$ in Fig. 6(a). Fig. 6(b) shows the perturbation energy $E(v)$ and the control effort $C(v) = \frac{1}{d}\int_0^d v(x,-1,t)^2 + v(x,1,t)^2\mathrm{d}x$, for magnetic fields of different strength. The ratio between the kinetic energy of the boundary control flow and the perturbation kinetic energy, $C(v)/E(v)$, is less than 1%, which suggests that small control can result in considerable mixing effect. Fig. 7 shows the evolution in time of $m(\mathbf{v}, \mathbf{B})$, our mixing measurement. In Fig. 7, the magnetic field is imposed at $t = 0$ with the fully established flow (R $= 7500$) achieved in Fig. 4 for the pure hydrodynamic channel. The controller is started at around $t = 6000$ with the fully established flow (R $= 7500$, $R_m = 0.1$, N $= 0.01$) achieved in Fig. 5(a). We can observe once again the negative and positive effect on mixing produced by the magnetic field and the boundary control respectively. An intuitive representation of the control mechanism in this case can be seen from the boundary zoom-in (Fig. 8). The velocity vectors show that boundary control is pushing, by blowing, the nearby vortex into the center of the flow.

The mixing governed by the stretching and folding of material elements, as the one considered in this work, can be determined by studying the movement of a passive tracer, or dye, in a homogeneous fluid flow. The location of the dye as a function of time completely describes the mixing. A particle tracking analysis is carried out to further visualize the mixing effectiveness of the

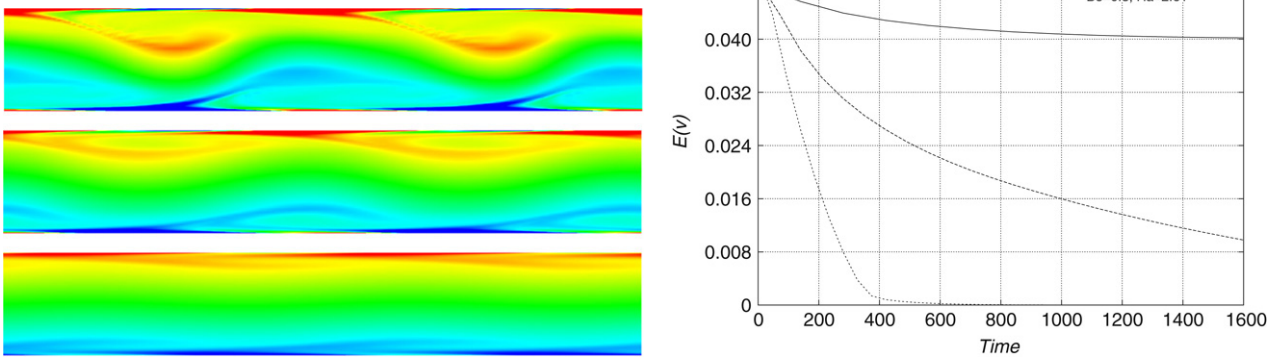


(a) Flow being stabilized by magnetic field ($B_0 = 0.3$, $t = 140, 285, 374$).

(b) Perturbation energy as function of time ($B_0 = 0.1, 0.2, 0.3$).

**Fig. 5.** Uncontrolled flow at $R = 7500$, $R_m = 0.1$, $N = 0.01$.

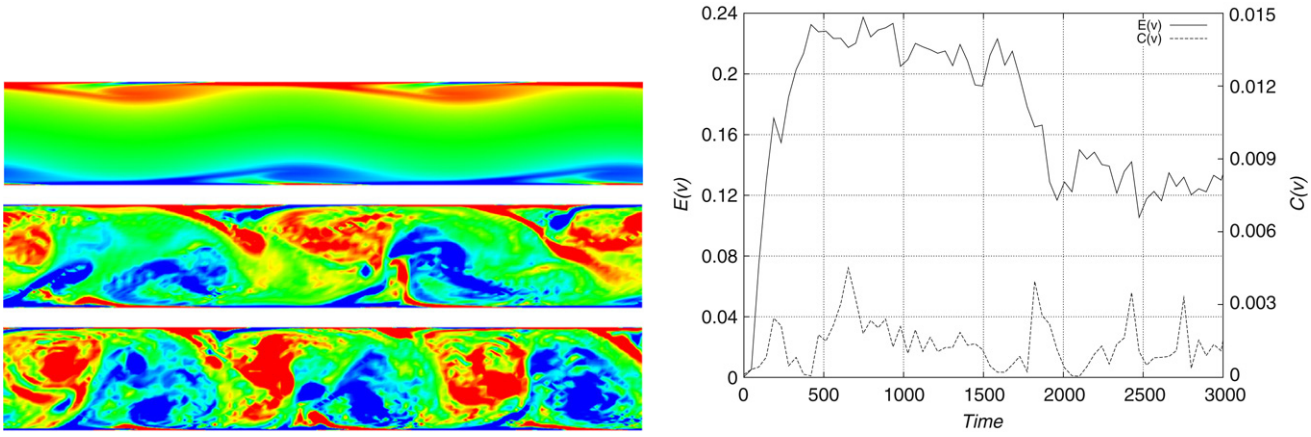


(a) Flow being destabilized by boundary control ($B_0 = 0.3$, $t = 47, 140, 327$).

(b) Perturbation energy and control effort as functions of time ($B_0 = 0.3$).

**Fig. 6.** Controlled flow at $R = 7500$, $R_m = 0.1$, $N = 0.01$.

**Fig. 7.** Evolution of $m(\mathbf{v}, \mathbf{B})$ ($R = 7500$, $R_m = 0.1$, $N = 0.01$, $B_0 = 0.3$).

control law. At $t = 0$ several blobs are distributed along the centerline of the channel, concentrated on several circular regions, as shown in Fig. 9(a). The 100,000 particles used in this simulation study are assumed to exactly follow the fluid motion. Fig. 9(b) shows the evolution in time of the dye blobs in the uncontrolled case, whereas Fig. 9(c) shows the particle map evolution for the controlled flow. In both cases, the tracking starts with the fully established MHD flow ($R = 7500$, $R_m = 0.1$, $N = 0.01$, $B_0 = 0.3$) shown in Fig. 5(a). The difference in complexity between the uncontrolled and controlled cases is manifested.

**Fig. 8.** Controlled flow at $R = 7500$, $R_m = 0.1$, $N = 0.01$. Pressure and velocity zoom at the boundary ($B_0 = 0.3$).

## 8. Conclusions

Using the $L_2$-norm of first-order spatial derivatives of the velocity and magnetic field perturbations as a measure of mixing (that incorporates stretching and folding of material elements), a feedback law that maximizes this measure and minimizes the control and sensing efforts was designed for a 2D Hartman flow. The controller does not drive the states (or the control inputs) unbounded but it does locally destabilize the system, leading to bounded unsteadiness, and, indirectly, to enhanced mixing. The controller effectiveness is demonstrated in a full MHD code, showing flow patterns considerably more complex than in the fully established uncontrolled flow, despite a small control effort,